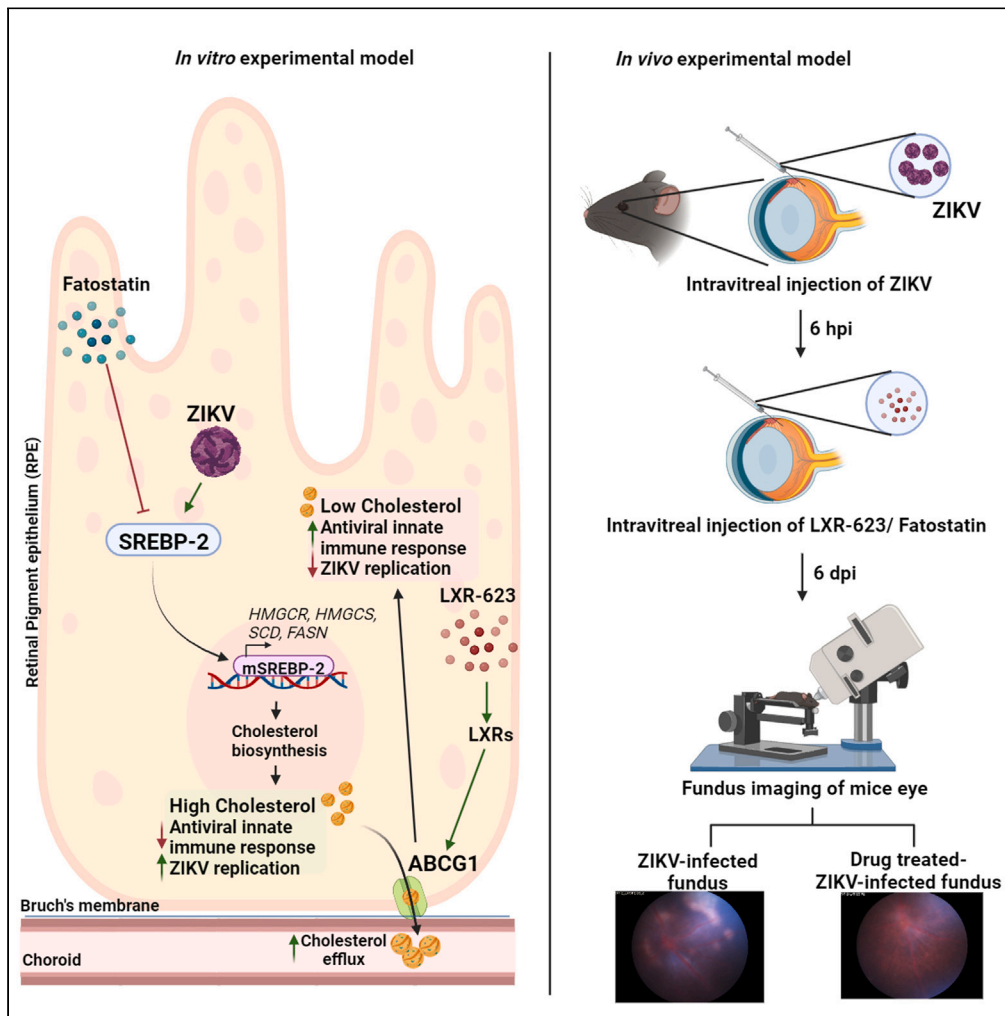## Article

Targeting ABCG1 and SREBP-2 mediated cholesterol homeostasis ameliorates Zika virus-induced ocular pathology

Sneha Singh, Robert E. Wright III, Shailendra Giri, Vaithilingaraja Arumugaswami, Ashok Kumar

akuma@med.wayne.edu

Highlights

Zika virus infection increases ABCG1 and SREBP-2 expression in RPE cells

ABCG1 deficiency reduces antiviral response and enhances ZIKV replication

SREBP-2 inhibition reduces cholesterol levels and attenuates ZIKV replication

LXR-623 or fatostatin alleviated ZIKV-induced chorioretinal lesions in mice

Article

Targeting ABCG1 and SREBP-2 mediated cholesterol homeostasis ameliorates Zika virus-induced ocular pathology

Sneha Singh,[1] Robert E. Wright III,[1] Shailendra Giri,[2] Vaithilingaraja Arumugaswami,[3] and Ashok Kumar[1,4,5,*]

SUMMARY

Zika virus (ZIKV) infection during pregnancy causes severe neurological and ocular abnormalities in infants, yet no vaccine or antivirals are available. Our transcriptomic analysis of ZIKV-infected retinal pigment epithelial (RPE) cells revealed alterations in the cholesterol pathway. Thus, we investigated the functional roles of ATP binding cassette transporter G1 (ABCG1) and sterol response element binding protein 2 (SREPB-2), two key players in cholesterol metabolism, during ocular ZIKV infection. Our *in vitro* data showed that increased ABCG1 activity via liver X receptors (LXRs), reduced ZIKV replication, while ABCG1 knockdown increased replication with elevated intracellular cholesterol. Conversely, inhibiting SREBP-2 or its knockdown reduced ZIKV replication by lowering cholesterol levels. *In vivo*, LXR agonist or SREBP-2 inhibitor treatment mitigated ZIKV-induced chorioretinal lesions in mice, concomitant with decreased expression of inflammatory mediators and increased activation of antiviral response genes. In summary, our study identifies ABCG1's antiviral role and SREBP-2's proviral effects in ocular ZIKV infection, offering cholesterol metabolism as a potential target to develop antiviral therapies.

INTRODUCTION

Zika virus (ZIKV) is a mosquito-borne viral infection that belongs to the *Flaviviridae* family. Despite its first identification in 1947, it has mostly caused sporadic outbreaks in various parts of Africa and Asia. However, it gained international attention during a large outbreak in Brazil in 2015–16 when WHO declared it as a public health emergency. Since then ZIKV transmission has been reported in several countries at variable rates, indicating the need for continued surveillance to track disease and ensure preparedness for early detection and response. Over the last decade, extensive research efforts were made to better understand ZIKV, its transmission, and its impact on human health. Moreover, the COVID-19 pandemic and rapid deployment of its vaccine has propelled the vaccine development for other RNA viruses, including ZIKV, with several candidates under investigation. However, currently, there are no approved antiviral therapies or vaccines for ZIKV.

While the majority of ZIKV infections remain asymptomatic, the acute phase of infection is associated with mild fever, maculopapular rash, myalgia, joint pain, headache, and retro-orbital pain. These symptoms usually last for a few days to a week. However, one of the most concerning aspects of ZIKV infection is its association with congenital ZIKV syndrome in babies born to infected mothers during pregnancy. This syndrome can lead to severe birth defects, including microcephaly, brain damage, vision and hearing impairment, and other developmental issues. In adults, severe ZIKV infection can cause Guillain-Barre syndrome, a neurological disorder.[1–3] In the eye, ZIKV infection causes conjunctivitis, uveitis, maculopathy, macular edema, chorioretinal atrophy, hypertensive iridocyclitis, macular pigment mottling, iris coloboma along with changes in the retinal vasculature, and optic neuropathy.[4–10] However, the pathogenesis of these ocular complications of ZIKV remains elusive. Because of our interest in ocular infectious diseases, including those caused by RNA viruses (ZIKV and severe acute respiratory syndrome coronavirus 2 [SARS-CoV-2]), our laboratory has developed experimental models to study host-pathogen interactions in the eye.

Earlier, we reported that ZIKV infects the cells lining the blood-retinal barrier (BRB), composed of retinal pigment epithelial cells (RPE) and retinal vascular endothelial cells.[11,12] The BRB protects the eye from blood-borne pathogens, including ZIKV. To get better insights into the pathogenesis of ocular ZIKV infection,[13,14] we performed a transcriptome analysis of ZIKV-infected RPE cells. We observed that ZIKV alters various metabolic pathways, including those involved in energy metabolism, specifically glycolysis. Moreover, the meta-analysis of transcriptomic profiles of ZIKV-infected RPE and cells infected with DENV (Dengue virus), WNV (West Nile virus), JEV (Japanese encephalitis virus), and HCV (Hepatitis C virus), led to the identification of lipid/cholesterol metabolism as one of the key pathways impacted during ZIKV infection.[15]

[1]Department of Ophthalmology, Visual and Anatomical Sciences/ Kresge Eye Institute, Wayne State University School of Medicine, Detroit, MI, USA
[2]Department of Neurology, Henry Ford Health System, Detroit, MI, USA
[3]Department of Molecular and Medical Pharmacology, University of California, Los Angeles, Los Angeles, CA, USA
[4]Department of Biochemistry, Microbiology, and Immunology, Wayne State University School of Medicine, Detroit, MI, USA
[5]Lead contact
*Correspondence: akuma@med.wayne.edu
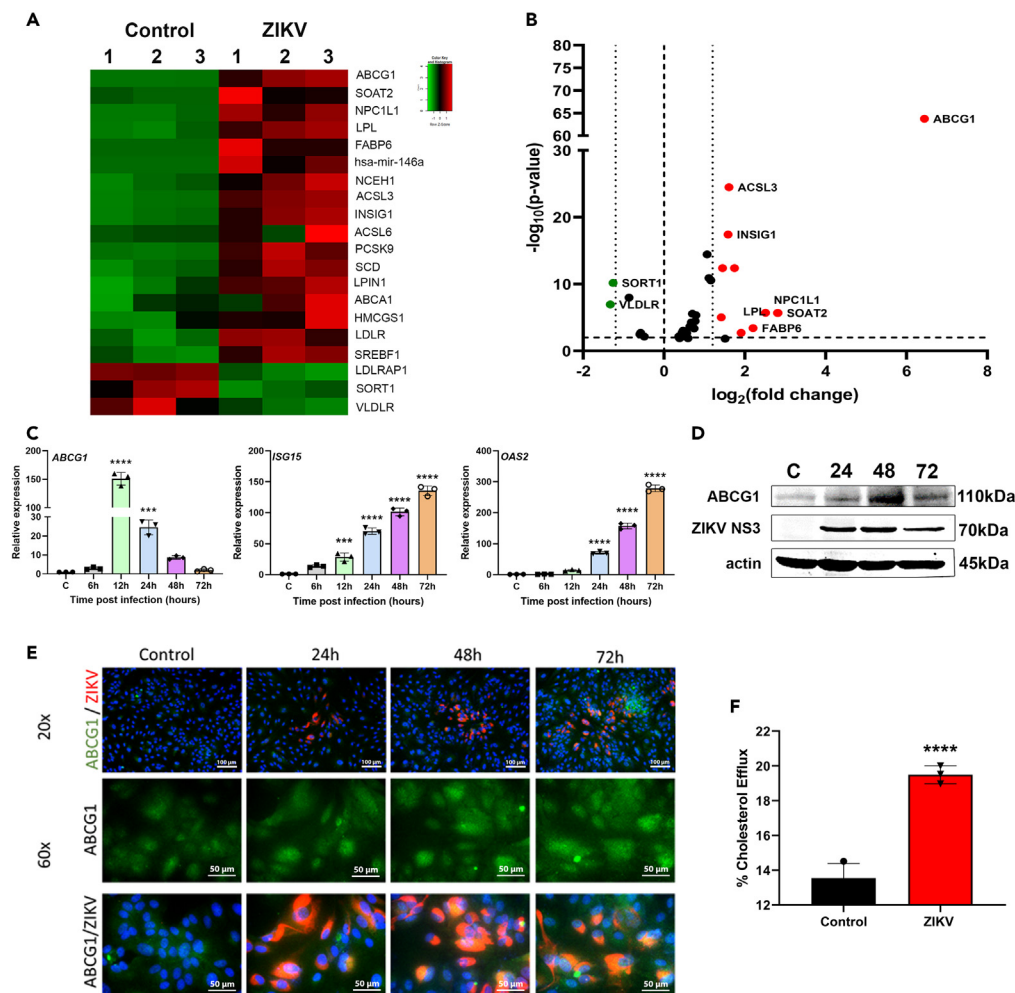https://doi.org/10.1016/j.isci.2024.109088

Figure 1. ZIKV infection upregulates ABCG1 expression and induces cholesterol efflux in RPE cells

human RPE (ARPE-19 cell line) cells infected with ZIKV strain PRVABC59 at MOI 1 for 48 h were subjected to RNAseq and heatmap (A) and volcano plot (B) were generated to visualize the expression pattern of genes regulating cholesterol and lipid metabolism. In another experiment, a time course study was performed by infecting RPE cells with indicated time points. The mRNA levels of the indicated genes were quantified using qPCR (C) whereas protein levels of ABCG1 and ZIKV viral protein NS3 were detected by western blotting (D). RPE cells were infected with ZIKV at MOI 1 for 48 h and immunostained for ZIKV envelope (red) and ABCG1 (green) and the nuclei were counterstained using DAPI (blue) and the images were captured at 20x and 60x magnification (E). The cell culture supernatant from mock-infected and ZIKV-infected RPE cells at 48 hpi was used for the estimation of cholesterol efflux expressed as percentage. Scale bar: 50 μm (F). The values represent mean $\pm$ SD from three independent experiments and the p value was calculated using one-way ANOVA with Dunnett's test. ****p < 0.0001, ***p < 0.001, **p < 0.01.

The host cell lipids and cholesterol play an essential role in various stages of viral replication, including entry, uncoating, assembly, and release.[16] However, the role of cholesterol metabolism in ZIKV infection remains elusive. In this study, we sought to investigate whether targeting ATP binding cassette transporter G1 (ABCG1) and sterol response element binding protein 2 (SREBP-2), the key genes involved in maintaining cholesterol homeostasis, modulates ZIKV-induced pathology in the eye.

RESULTS

ZIKV infection increases the expression of genes regulating cholesterol homeostasis

In our prior microarray study,[15] we reported that ZIKV readily infects human RPE and alters various metabolic pathways, including lipid metabolism. In this study, we performed RNAseq analysis (NCBI: PRJNA1032054) which further confirmed that genes/pathways regulating lipid and cholesterol metabolism were significantly upregulated in ZIKV-infected primary RPE cells (Figure 1A). Among the multiple genes, the expression of ABCG1, a cholesterol efflux transporter was the highest (Figure 1B), so we sought to investigate its role during ZIKV infection. First, we performed a time-course study and checked the expression pattern of *ABCG1* and other genes involved in innate antiviral response. Our data showed that ZIKV significantly upregulated the expression of *ABCG1* (~150-fold) at 12 h post-infection (hpi) followed by a gradual
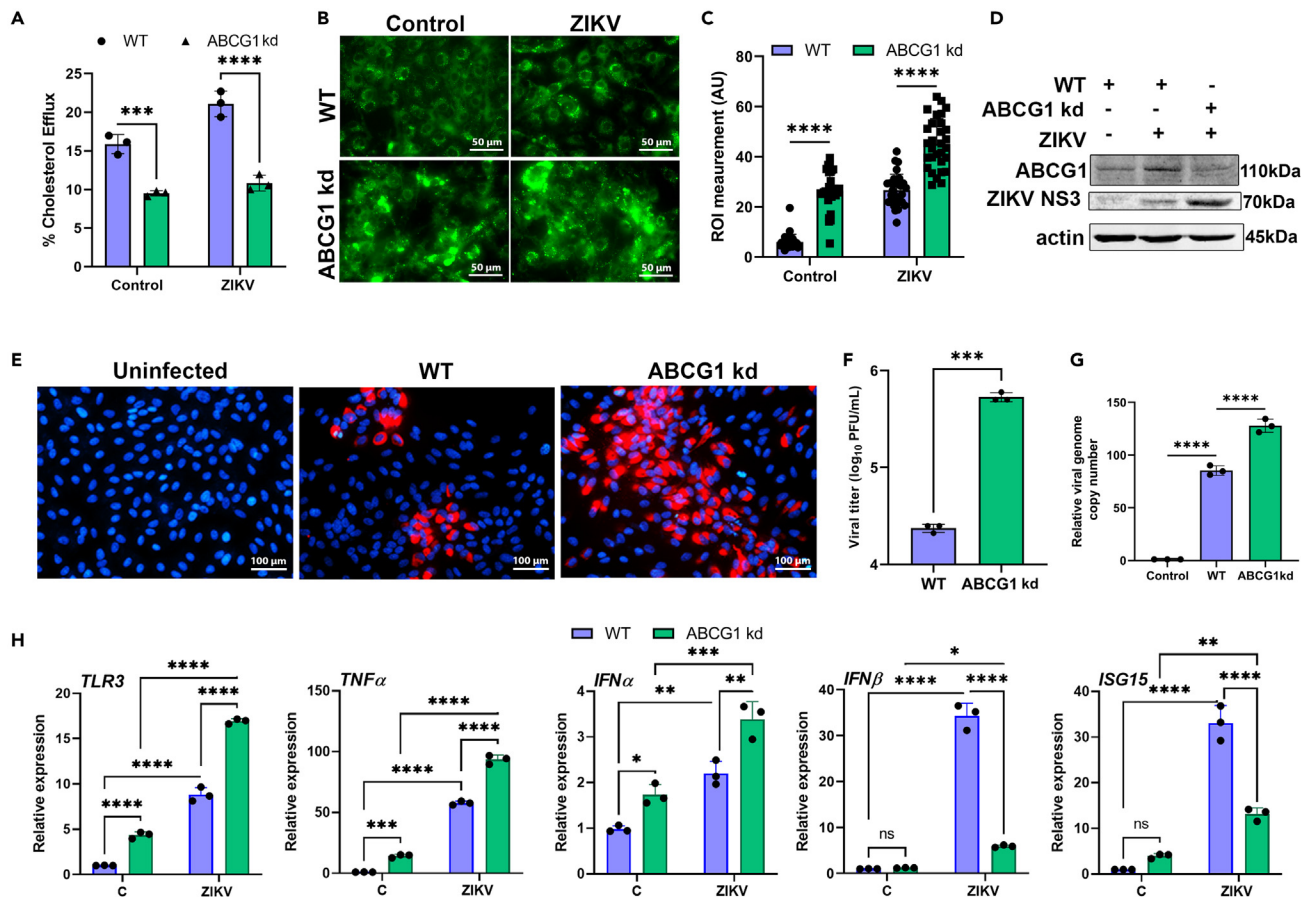
Figure 2. Knockdown of ABCG1 increases ZIKV replication and lipid droplet distribution in RPE cells

(A) ARPE-19 cells transduced with ABCG1-shRNA lentivirus were infected with ZIKV at MOI 1 for 48 h. The cell culture supernatant was collected and the cholesterol efflux was estimated and expressed as percentage age.

(B) Under similar experimental conditions, cells were live stained for lipid droplets (green) using a specific dye and visualized at 600x magnification. Scale bar: 50 μm.

(C) The intensity of lipid droplets was measured in each cell and represented as ROI measurement (arbitrary units, AU) using ImageJ software. (mean ± SD; n = 80)

(D) The whole cell lysates were used for immunoblot to assess the expression of ABCG1, ZIKV NS3, and actin.

(E) The cells were immunostained for ZIKV envelope (red) and the nuclei were counterstained using DAPI (blue), 200x magnification. Scale bar: 100 μm.

(F) The cell culture supernatant from the infected wild-type (WT) and ABCG1-shRNA transduced (ABCG1 kd) RPE cells were used for plaque assay to quantify the viral titer and expressed as PFU/mL on a logarithmic scale.

(G) qPCR was performed to quantify the relative expression of ZIKV RNA and (H) genes involved in pattern recognition (*TLR3*), inflammatory (*TNFα*), IFNs (*IFNα*, *IFNβ*), and IFN-inducible genes (*ISG15*). The values represent mean ± SD from three independent experiments, and the statistical analysis was performed using one-way ANOVA with Tukey's test. ****$p < 0.0001$, ***$p < 0.001$.

decline until 72 hpi. However, the expression of genes regulating the antiviral response (e.g., *ISG15* and *OAS2*) showed a time-dependent increase (Figure 1C), concomitant with temporal ZIKV replication as reported in our previous study.[13] The expression of ABCG1 at the protein level was induced at 24 hpi but mainly elevated at 48 hpi coinciding with increased viral replication indicated by viral NS3 protein levels (Figure 1D). These results were further confirmed by immunofluorescence assay wherein, the expression of ABCG1 increased in ZIKV-infected RPE cells in a time-dependent manner (Figure 1E). Since ABCG1 is involved in the efflux of cholesterol outside the cell, we performed cholesterol efflux assay using a kit-based method. We observed that ZIKV-infected RPE had a relatively higher percentage of cholesterol in the culture supernatant (Figure 1F). Overall, these results show that ZIKV infection induces the expression of ABCG1 and increases cholesterol efflux in RPE cells.

ABCG1 knockdown or inhibition promotes ZIKV infection and reduces antiviral response

Previously, we reported that cholesterol supplementation enhances ZIKV infection, indicating its proviral role. Since ABCG1 regulates cholesterol efflux, we hypothesized that increased ABCG1 activity during ZIKV infection will reduce the availability of intracellular cholesterol resulting in reduced viral replication.[17] To test our hypothesis and to determine the specific role of ABCG1 on ZIKV infection, we performed

shRNA-lentivirus-induced knockdown (KD) of ABCG1 in RPE cells. Our data showed that cholesterol efflux was significantly reduced in both mock and ZIKV-infected ABCG1 knockdown cells whereas expected the cholesterol efflux was higher in ZIKV-infected wild-type (WT) cells (Figure 2A). Moreover, ABCG1 knockdown increased lipid droplets in the mock and ZIKV-infected cells (Figure 2B), indicating the intracellular accumulation of lipid/cholesterol contents (Figure 2C). The western blot analysis revealed that ABCG1 protein levels were significantly reduced in ABCG1 knockdown RPE cells with a corresponding increase in NS3 levels, indicating more ZIKV infection (Figure 2D). These results were further confirmed by immunofluorescence staining (Figure 2E), plaque assay (Figure 2F), and viral RNA copy number (Figure 2G) showing increased ZIKV replication in ABCG1 knockdown cells. Together, these results indicate an antiviral role of ABCG1 against ZIKV.

The excessive accumulation of cholesterol or hypercholesteremia alters immune response with abrogated TLRs, pro-inflammatory cytokines, and reduced interferon response.[18] Hence, we evaluated the effect of ABCG1 knockdown on ZIKV-induced innate antiviral response. We performed qPCR analysis of viral recognition receptors (TLR3, RIG-I, MDA5), inflammatory mediators (TNFα, CXCL10, CCL5), interferons (IFNs) (IFNα, IFNβ, IFNγ), and IFN-inducible genes (OAS2, ISG15, MX1). Our data showed that ZIKV infection increased the expression of these innate inflammatory and antiviral response genes in WT RPE cells. However, in ABCG1 knockdown cells, the overall expression of inflammatory mediators increased whereas except IFNα, antiviral response declined, in response to ZIKV infection (Figures 2H and S1). Thus, these findings implicate ABCG1 in regulating innate antiviral response in RPE during ZIKV infection.

Because the ABCG family of transporters is involved in maintaining cholesterol homeostasis in the retina, their direct knockdown or inhibition under normal physiological conditions might be detrimental. As the liver X receptor (LXR) pathway is integral to regulating lipid metabolism and inflammatory signaling,[19] upon excessive cholesterol accumulation, LXRs get activated to promote cholesterol efflux by regulating the expression of ABCG1 and ABCA1. Thus, we sought whether the LXR pathway can be targeted to modulate ABCG1 expression and its antiviral properties by using LXR agonist (LXR-623) and LXR antagonist (SR-9238),[20,21] which did not exhibit cytotoxicity at the used concentrations (Figure S4). Treatment of ZIKV-infected cells with LXR-623 significantly reduced ZIKV infection (Figure 3A) and viral progeny production (Figure 3B). However, antagonist (SR-9238) treatment alone did not significantly affect viral replication but attenuated the antiviral effects of LXR-623 resulting in reduced cellular infectivity and viral titers.

To confirm whether the antiviral activity of LXR-623 against ZIKV infection is mediated via ABCG1, LXR-623 treatment was performed in ABCG1 knockdown cells followed by immunofluorescence staining of viral antigen and plaque assay. Our data showed that LXR-623-treated ABCG1 knockdown cells exhibited higher ZIKV infection (Figure 3C) and increased production of viral progeny (Figure 3D). Collectively, these observations indicated that LXR agonist exerts antiviral activity against ZIKV via enhancing ABCG1-mediated cholesterol efflux (Figure 3E).

ZIKV infection induces cholesterol synthesis to support viral replication

The cholesterol homeostasis in the cells is tightly regulated by its synthesis, extracellular uptake, and efflux of excess cholesterol. As our transcriptome analysis indicated an alteration in cholesterol metabolism, we assessed the effect of ZIKV infection on cholesterol synthesis in RPE cells. First, we checked the expression of genes encoding key enzymes regulating lipid and cholesterol synthesis (Figure 4A). Our data showed that ZIKV induced the temporal expression of HMGCR (HMG-CoA reductase), HMGCS (3-hydroxy-3-methylglutaryl-CoA synthase), SCD (stearoyl-coa desaturase), and FASN (fatty acid synthase) (Figure 4B). This response coincided with increased accumulation of lipid droplets in ZIKV-infected RPE cells with relatively higher levels at 48 and 72 hpi (Figure 4C). The intracellular levels of cholesterol are regulated by sterol sensors, such as the SREBP-2. We observed that ZIKV induced the expression of SREBP-2 as evidenced by immunofluorescence (Figure 4D) and western blot (Figures 4E and 4F) analyses. Overall, these results indicate that ZIKV infection enhances cholesterol synthesis.

Earlier, we reported that cholesterol supplementation increased ZIKV replication in RPE.[15] Thus, we hypothesized that inhibition of SREBP-2 activity would decrease cholesterol levels, resulting in reduced ZIKV replication. To test our hypothesis, we used fatostatin, a pharmacological inhibitor of both SREBP-1 and SREBP-2.[22] Moreover, fatostatin is known to exert anti-inflammatory effects without affecting cell viability.[23] Our data showed that fatostatin reduced ZIKV-induced SREPB-2 levels in RPE. NS3 viral proteins were also drastically reduced in fatostatin-treated ZIKV-infected cells (Figure 5A). Moreover, fatostatin treatment reduced the expression of cholesterol synthesis genes (Figure 5B). Furthermore, immunofluorescence (Figure 5C) and plaque assay (Figure 5D) revealed a significant reduction in viral replication as well as viral progeny production by fatostatin treatment. Interestingly, fatostatin treatment increased the expression of viral recognition receptors (TLR3, RIG-I, MDA5), IFNs (IFNα, IFNβ, IFNγ), and IFN-inducible genes (OAS2, ISG15, MX1) whereas the inflammatory genes (TNFα, CXCL10, CCL5) were significantly reduced (Figures 5E and S2). It is important to note that fatostatin at the used concentrations did not cause cytotoxicity (Figure S4). These results indicate that inhibition of SREBPs reduces ZIKV replication and enhances antiviral innate immune response in RPE cells.

SREBP-2 knockdown attenuates ZIKV replication in RPE cells

The aforementioned results demonstrated a reduction in ZIKV replication, in part by reducing cholesterol synthesis using a well-studied SREBP inhibitor, fatostatin. Therefore, to specifically investigate the role of SREBP-2 in ZIKV infection, we used a lentivirus-mediated knockdown approach. We observed that the knockdown of SREBP-2 resulted in significantly reduced puncta of lipid droplets in the mock-infected as well as ZIKV-infected RPE cells (Figure 6A). The knockdown of SREBP-2 was confirmed by western blotting showing a reduction in SREBP-2 and NS3 levels (Figure 6B). Similarly, SREBP-2 knockdown in RPE exhibited reduced ZIKV replication and progeny production as evidenced by immunofluorescence staining for viral envelope protein (Figure 6C) and plaque assay (Figure 6D). The assessment of antiviral innate response revealed results consistent with fatostatin treatment, SREBP-2 knockdown resulted in attenuation of inflammatory mediators (TNFα, CXCL10, CCL5) and elevated levels of antiviral response genes e.g., OAS2, ISG15, MX1, IFNα, IFNβ, and IFNγ (Figures 6E and S3). Collectively, these findings indicate a proviral role of SREBP-2 during ZIKV infection.
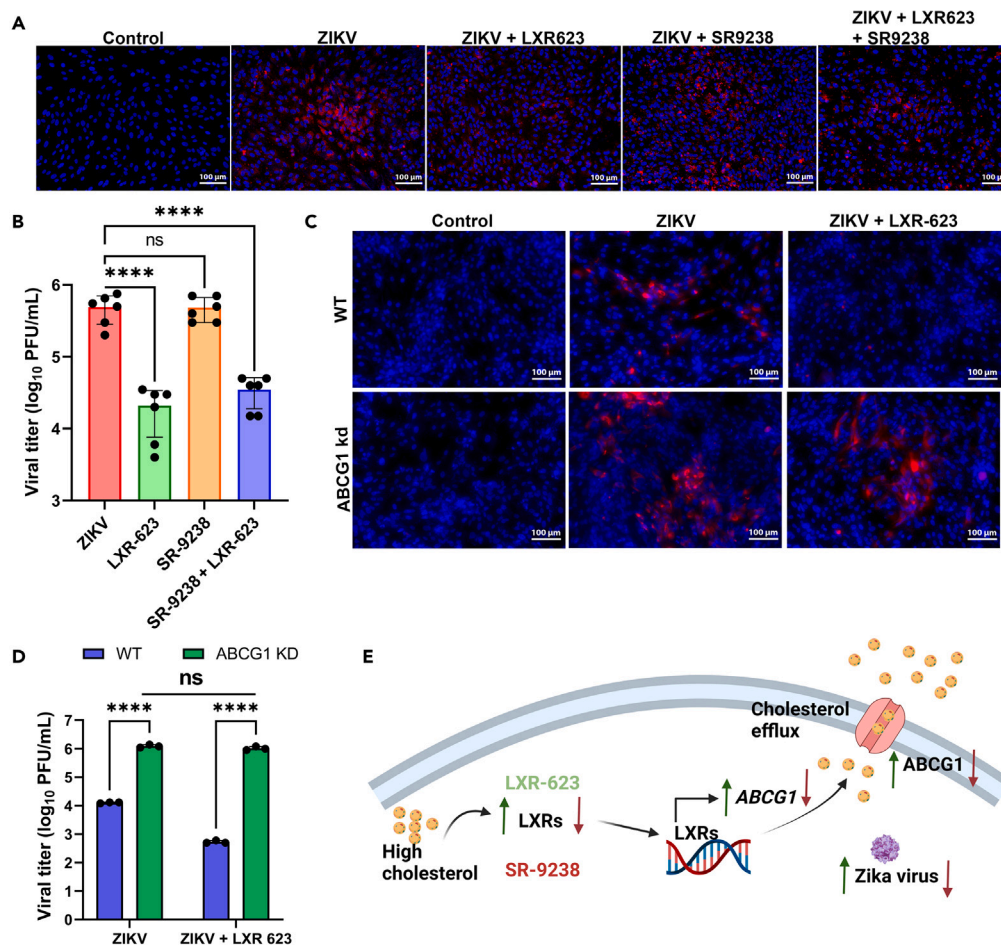
Figure 3. Pharmacological inhibition of ABCG1 promotes ZIKV replication in RPE cells

(A) RPE cells were infected with ZIKV at MOI 1 for 48 h in the presence or absence of LXR agonist (LXR-623) and inverse agonist (SR-9238). The cells were immunostained for ZIKV envelope 4G2 (red), and the nuclei were counterstained using DAPI (blue), 200x magnification. Scale bar: 100 μm.

(B) Culture supernatants were collected, and viral titers were estimated by plaque assay. The values were plotted on a logarithmic scale (mean ± SD; n = 6).

(C) ARPE-19 (WT) and ABCG1-shRNA transduced (ABCG1 kd) cells were infected with ZIKV at MOI 1 and treated with LXR-623✕and immunostained for ZIKV envelope (red) and the nuclei were counterstained using DAPI (blue), 200x magnification. Scale bar: 100 μm.

(D) The WT and ABCG1kd RPE cells were infected with ZIKV and treated with LXR-623 followed by plaque assay to quantify progeny virions expressed as $\log_{10}$ PFU/mL (mean ± SD; n = 3).

(E) A schematic representation of the effect of LXR on the expression of ABCG1, cholesterol efflux, and ZIKV replication was created using BioRender. The values represent mean ± SD from three independent experiments, and the statistical analysis was performed using one-way ANOVA with Tukey's test. ****$p < 0.0001$, ns, non-significant.

Fatostatin and LXR-623 ameliorate ZIKV-induced ocular pathology in mice

Our *in vitro* studies show that both SREBP inhibitor, fatostatin, and LXR agonist, LXR-623, restricted ZIKV replication in RPE cells. To determine their *in vivo* therapeutic effects, we employed a mouse model of ZIKV-induced chorioretinal atrophy by intravitreal administration of drugs 6 h post-ZIKV infection (Figure 7A). As anticipated, fundus imaging showed the development of chorioretinal lesions in ZIKV-infected C57BL/6 mice eyes whereas the mock-infected eyes had clear fundus.[13] In contrast, eyes treated with either LXR-623 (30 μM/eye) or fatostatin (15 μM/eye) had reduced lesions (Figure 7B). The viral copy number also decreased in eyes treated with fatostatin or LXR-623 as compared ZIKV-infected untreated group (Figure 7C). The qPCR analysis of retinal tissue showed upregulation of antiviral response genes *Isg15* and *Oas2* and a reduction in *Ccl5* expression in the treatment group (Figure 7D). Collectively, these findings indicate that the inhibition of cholesterol synthesis or induction of cholesterol efflux reduces ZIKV-induced ocular pathology.

DISCUSSION

Systemic viral infections cause vision impairment by disrupting the BRB, leading to infiltration of immune cells and intraocular inflammation. The RPE cells forming the outer BRB are the primary target of blood-borne viral pathogens. Therefore, in addition to their barrier properties,
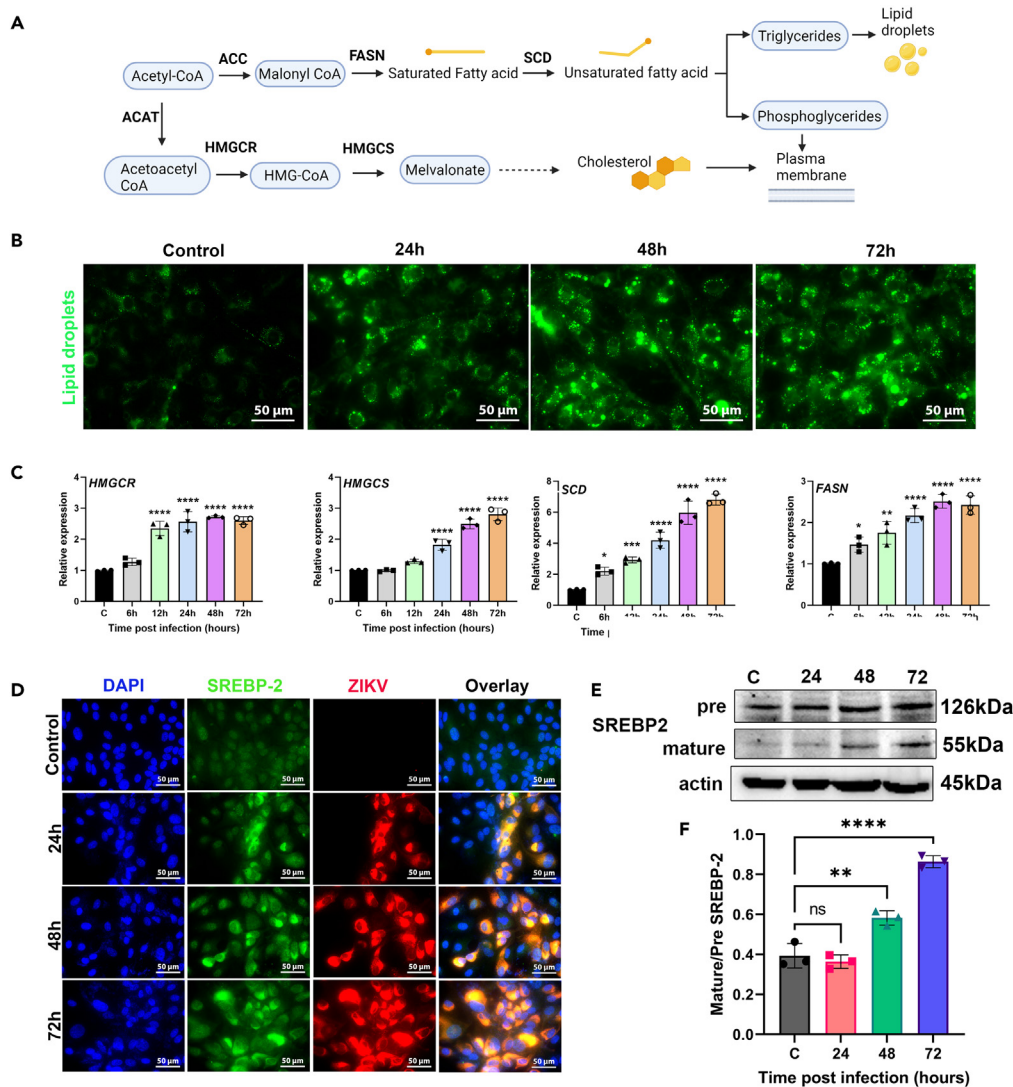
Figure 4. ZIKV infection increases cholesterol biosynthesis and induces SREBP-2 expression in RPE

(A) Schematic of genes/enzymes involved in cholesterol/lipid pathways.

(B) ARPE-19 cells were infected with ZIKV at MOI 1 for different time points. The cells were live stained for lipid droplets (green), 600x magnification. Scale bar: 50 μm.

(C) The mock-infected and ZIKV-infected cells were collected in Trizol for RNA isolation at different time points. cDNA was prepared for qPCR analysis of cholesterol biosynthesis genes (*HMGCR*, *HMGCS*, *SCD*, *FASN*).

(D) The cells were mock-infected or ZIKV-infected at different time points. The cells were fixed and immunostained for SREBP-2 (green) and ZIKV envelope 4G2 (red) while the nuclei were counterstained using DAPI (blue), 600x magnification. Scale bar: 50 μm.

(E) The whole cell lysate of mock-infected (C) and ZIKV-infected RPE cells at different time points post-infection was immunoblotted for SREBP-2 premature (pre), mature, and actin.

(F) The expression levels of mature/pre SREBP-2 were quantified by densitometry and plotted. Band densities of the mature and pre-SREBP-2 proteins were normalized to the respective loading control, β-actin. The values represent mean $\pm$ SD (n = 3), and the statistical analysis was performed using one-way ANOVA with Tukey's test. ns non-significant, ****$p < 0.0001$, ***$p < 0.001$, **$p < 0.01$, *$p < 0.05$.

RPE cells orchestrate both, innate and adaptive responses during infection, autoimmunity, and retinal degeneration.[24] The high permissiveness of RPE to ZIKV makes it an appropriate cell type to study host-virus interactions in the eye.[13,15,25] Here, using both *in vitro* and *in vivo* models of ZIKV infection and pharmacological inhibitors and gene knockdown approaches, we report that cholesterol metabolism regulates ZIKV replication and host antiviral response in RPE cells. Together, our study demonstrates that ABCG1-mediated cholesterol efflux exerts antiviral effects whereas increased SREBP-2 activity promotes viral replication.
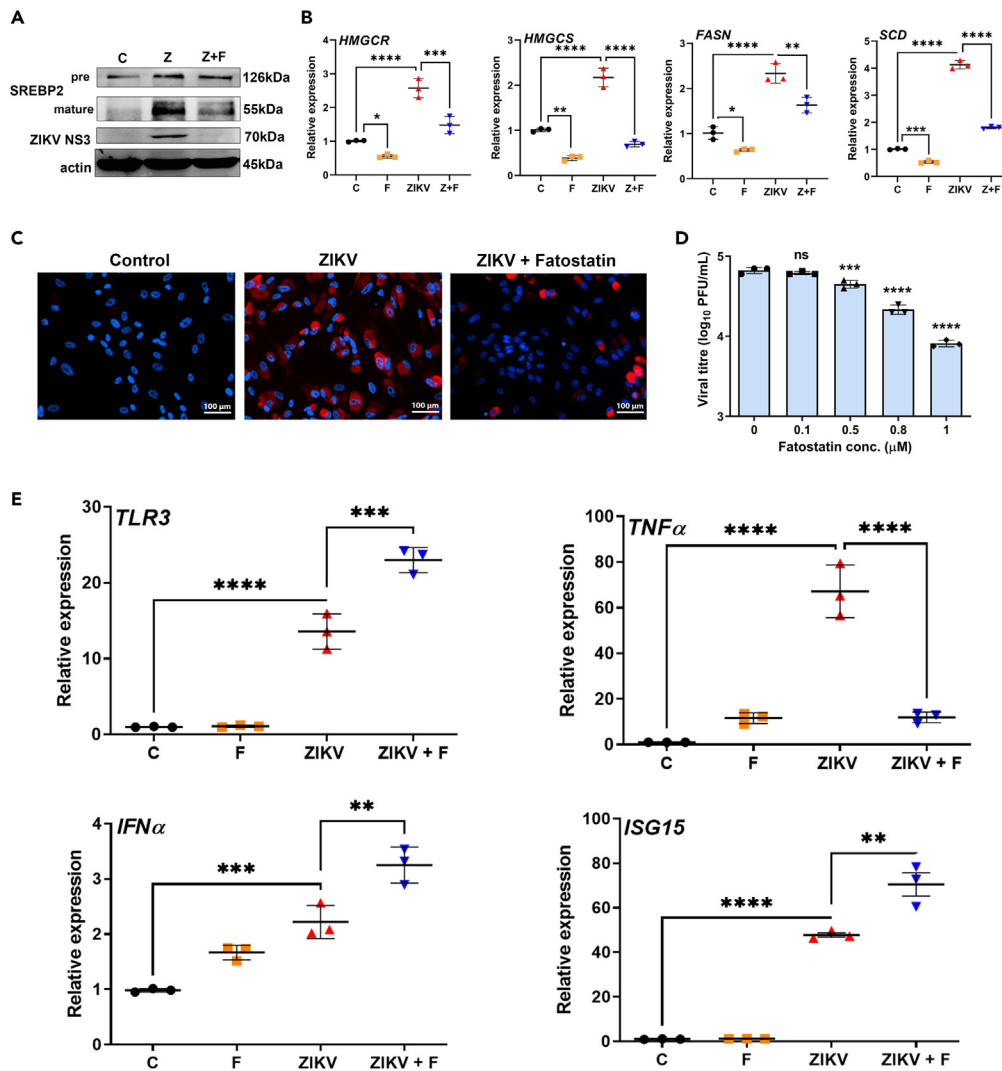
Figure 5. Inhibition of SREBP-2 reduces ZIKV replication and induces antiviral innate immune response

(A) ARPE-19 cells were mock-infected or infected with ZIKV at MOI 1 for 48 h and treated with 1μM of fatostatin (F). The whole cell lysate was used for the western blot detection of SREBP-2 precursor (pre) and mature protein, ZIKV NS3, and actin.

(B) Under similar conditions, the cells were collected in Trizol for RNA isolation and cDNA preparation followed by qPCR analysis of cholesterol biosynthesis genes (*HMGCR*, *HMGCS*, *SCD*, and *FASN*).

(C) The cells were immunostained for ZIKV envelope 4G2 antigen (red) and the nuclei were counterstained using DAPI. Scale bar: 100 μm.

(D) The cells were infected with ZIKV at MOI 1 for 48 h and treated with varying concentrations of fatostatin. The cell culture supernatant was used to perform plaque assay and viral titer was expressed on a logarithmic scale as PFU/mL.

(E) qPCR was performed to quantify the relative expression of genes involved in pattern recognition (*TLR3*), inflammatory (*TNFα*), IFNs (*IFNα*), and IFN-inducible genes (*ISG15*). The values represent mean $\pm$ SD (n = 3), and the statistical analysis was performed using one-way ANOVA with Tukey's test. ns non-significant, ****$p < 0.0001$, ***$p < 0.001$, **$p < 0.01$, *$p < 0.05$.

Cholesterol is a vital ingredient for the replication of flaviviruses within the host cells. Thus, host cholesterol metabolism can potentially modulate ZIKV replication.[26–30] Our meta-analysis of transcriptomic profiles of ZIKV, DENV, JEV, WNV, and HCV indicated the dysregulation of lipid metabolic pathways with a significant alteration of *ABCG1*, as one of the ZIKV-core signature genes.[15] ABCG1 is localized on the endoplasmic reticulum (ER) as well as the plasma membrane of the cells[31,32] involved in cellular lipid transport and cholesterol homeostasis. However, there is limited knowledge on the role of ABCG1 in the context of viral replication and host immune response. Our data showed an increased level of ABCG1 expression as well as cholesterol efflux in ZIKV-infected RPE cells. ABCG1 expression has been shown to limit the replication of enveloped RNA viruses due to cholesterol efflux from intracellular compartments and interference with the viral replication and assembly process.[33,34] Thus, we hypothesize that increased cholesterol efflux upon ZIKV infection might be a defense mechanism of RPE cells to deplete cholesterol, an essential ingredient for the formation of viral replication complexes (VRCs) during flavivirus infection.[35,36]
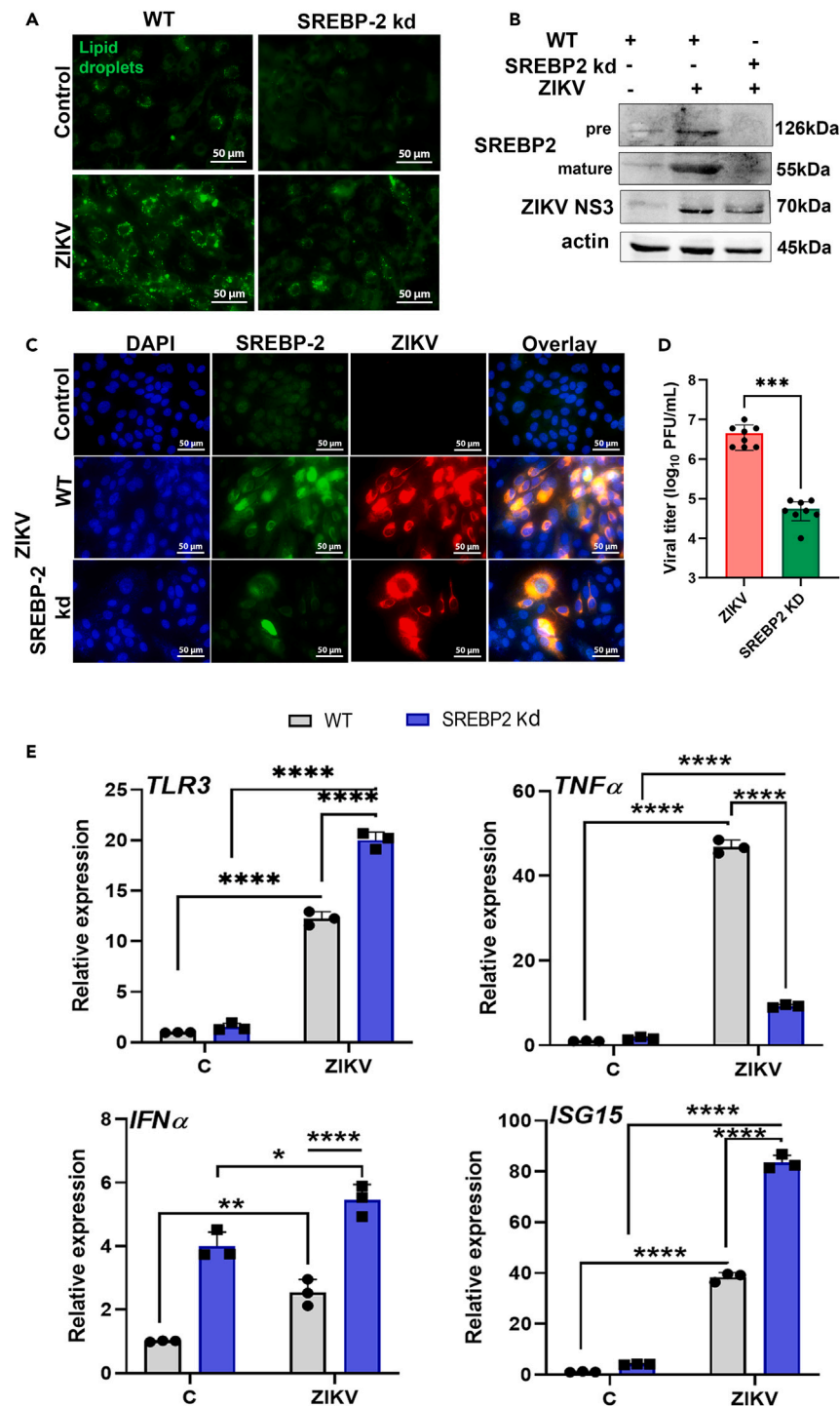
Figure 6. SREBP-2 knockdown reduces cholesterol synthesis and ZIKV replication in RPE cells

(A) ARPE-19 cells transduced with SREBP-2-shRNA lentivirus and mock-treated (WT) cells were infected with ZIKV at MOI 1 for 48 h. The lipid droplets were live stained and the images were visualized at 600x magnification. Scale bar: 50 μm.

(B) Under similar conditions, the whole cell lysate was collected in RIPA buffer and immunoblotted for SREBP-2 precursor (pre) and mature SREBP-2, ZIKV NS3, and actin.

(C) The cells were fixed and immunostained for SREBP-2 (green), ZIKV envelope antigen (red) while the nuclei were counterstained using DAPI (blue), 600x magnification. Scale bar: 50 μm.

Figure 6. Continued

(D) The cell culture supernatant from the SREBP-2 kd and mock-infected wild-type (WT) cells were used for plaque assay. The viral titer was expressed on a logarithmic scale of PFU/mL.

(E) qPCR was performed to quantify the relative expression of genes involved in pattern recognition (*TLR3*), inflammatory (*TNFα*), IFNs (*IFNα*), and IFN-inducible genes (*ISG15*). The values represent mean ± SD (n = 8), and the statistical UTR analysis was performed using one-way ANOVA with Tukey's test. ***p < 0.001.

The *de novo* synthesis, import and export of cholesterol are tightly regulated to control the intracellular cholesterol levels wherein a key transcription factor to regulate cholesterol homeostasis is the LXRs targeting ABCG1 and ABCA1.[37–39] Agonists of LXRs have been shown to attenuate RNA virus replication (HCV, HIV, POWV (Powassan virus), ZIKV, and CHIKV (Chikungunya virus)) via upregulation of ABCG1 and/or ABCA1 expression.[40,41] The LXR pathway is known to modulate lipid metabolism and innate immune response along with the reduction of inflammation in multiple human and mouse cells.[42,43] Likewise, our results demonstrate that induction of LXRs attenuates ZIKV replication in RPE cells and mice retinal tissue which corroborates with a recent study wherein ZIKV infection in human neuroblastoma cells was inhibited by LXR-623.[41] However, unexpectedly LXR antagonist SR-9238 did not increase ZIKV infection in the presence of LXR-623. The observed effect could be due to its cell or tissue specific action of SR-9238 in activating LXRs such as those expressed in liver hepatocytes vs. peripheral LXRs in retinal cells.[21,44]

Our transcriptomic study showed the upregulation of ABCG1 with no significant alteration in ABCA1 expression in ZIKV-infected RPE. Therefore, we hypothesized that the antiviral effect of LXR agonist against ZIKV is likely to be mediated via ABCG1. This was supported by our data showing increased ZIKV replication in LXR-623-treated ABCG1 knockdown cells. Our results show that the knockdown of ABCG1 correlated with higher ZIKV replication due to the increased availability of cholesterol-loaded lipid droplets to form viral replication complexes (VRCs). Our study demonstrates that ZIKV induces the expression of ABCG1 and cholesterol efflux and the use of LXR agonist to boost ABCG1 attenuates ZIKV replication. Therefore, pharmacological stimulation of cholesterol efflux can be considered as an anti-ZIKV therapeutic strategy. We observed that ABCG1 knockdown attenuated ZIKV-induced expression of antiviral immune response genes but increased levels of inflammatory genes. Although the underlying mechanism of this differential innate response needs further investigation, the reduction in antiviral molecules (e.g., ISG15) might have contributed to enhancing ZIKV replication whereas elevated inflammatory mediators can cause retinal cell death. Among the antiviral molecules, the expression pattern of IFNα was opposite i.e., its levels increased in ABCG1 deficient cells, indicating its ABCG1 independent modulation. The higher levels of inflammatory mediators, in ABCG1 deficient RPE could be due to increased accumulation of intracellular cholesterol. Studies have shown that flavivirus non-structural proteins inhibit type I IFN response to facilitate their replication and high cholesterol promotes poor IFN response.[17,18] Thus, reduction of cholesterol levels during ZIKV infection could enhance IFN response resulting in a decreased ZIKV infectivity as evident in ABCG1 knockdown RPE cells. These results indicate an antiviral role of ABCG1 expression in RPE and warrant further investigations to target the cholesterol efflux pathway during viral infection.

The cholesterol biosynthesis pathway is a complex series of enzymatic reactions and forms a crucial part of cholesterol homeostasis in the cells. SREBP-2 is a key transcription factor and a master regulator of cholesterol homeostasis[45–47] and plays a central role in coordinating the expression of genes involved in cholesterol synthesis including HMG-CoA reductase (HMGCR). SREBP-2 activation has been linked to induced expression of ISGs while its inhibition attenuates flavivirus (HCV, DENV, and ZIKV) replication.[45,48–51] However, the crosstalk between SREBP-2 and antiviral immune response during flavivirus infection has not been studied in depth. HCV and HIV increase the expression and proteolytic activation of SREBP-1 and SREBP-2, promoting cholesterol synthesis and facilitating viral replication. Our data showed that ZIKV infection of RPE causes lipid accumulation and increased expression of genes regulating cholesterol biosynthesis like other flaviviruses.[45,51–53] The inhibition of ZIKV replication has been shown using SREBP inhibitors—nordihydroguaiaretic acid (NDGA), and its methylated derivative tetra-*O*-methyl nordihydroguaiaretic acid (M4N), PF-429242, DMHCA, and fatostatin.[51,54] Similarly, we found that inhibition of SREBPs increases IFNs and ISGs which contribute to resistance against ZIKV infection whereas reduced inflammatory cytokines aid in attenuating virus-induced cytopathic effects. The reduction in cholesterol levels during flavivirus infection enhances the IFN response.[18] Moreover, SREBP-2 can modulate the transcription of genes encoding antiviral response including TLRs, pro-inflammatory cytokines, and chemokines.[47,55] The HCV viral proteins (Core, NS4B, NS5A) and 3′ UTR have been found to activate the SREBP signaling pathway and induce lipid biosynthesis.[45] The involvement of specific ZIKV proteins in modulating the SREBP pathway needs to be further studied. During DENV infection, cholesterol synthesis is increased via upregulation of HMGCR and downregulation of AMP-activated protein kinase (AMPK).[56,57] Moreover, apart from statins, metformin, a drug commonly used to treat diabetes, also inhibits the cholesterol synthesis enzyme, HMGCR.[58] We showed that metformin reduces ZIKV infection by activation of AMPK, a sensor of cellular energy, as an alternative to inhibit cholesterol synthesis.[17,59] In our previous study, we reported that ZIKV infection of retinal endothelial cells reduces AMPK as well as ACC (acetyl CoA carboxylase) levels, which otherwise would increase lipid and cholesterol synthesis via increased SREBP-2 activity.[59] Therefore, modulating SREBP-2 activity can be harnessed as a therapeutic strategy against enveloped viral infections.

The lipid homeostasis and antiviral response against enveloped RNA viruses is not well studied with several open questions to be explored. Several human miRNAs (miR24, miR33, miR148a, and miR29) have been known to regulate lipid metabolism including the ABCG1/ABCA1 pathway and SREBP pathway wherein their role in altering ZIKV and other enveloped RNA virus replication needs to be explored for therapeutic antiviral manipulation.[28,45,60] Also, in COVID-19 patients, SREBP-2 is highly activated with an elevated level of circulating SREBP-2 C-terminal fragment. This raises the possibility of whether SREBP-2 levels can be used to gauge the severity of RNA virus infection.[61] SREBP-2 and ABCG1 have an intricate relationship in regulating cholesterol metabolism[39] and SREBP-2 activation increases the expression of ABCG1 in macrophages and other cell types suggesting that SREBP-2 may directly promote cholesterol efflux via ABCG1,
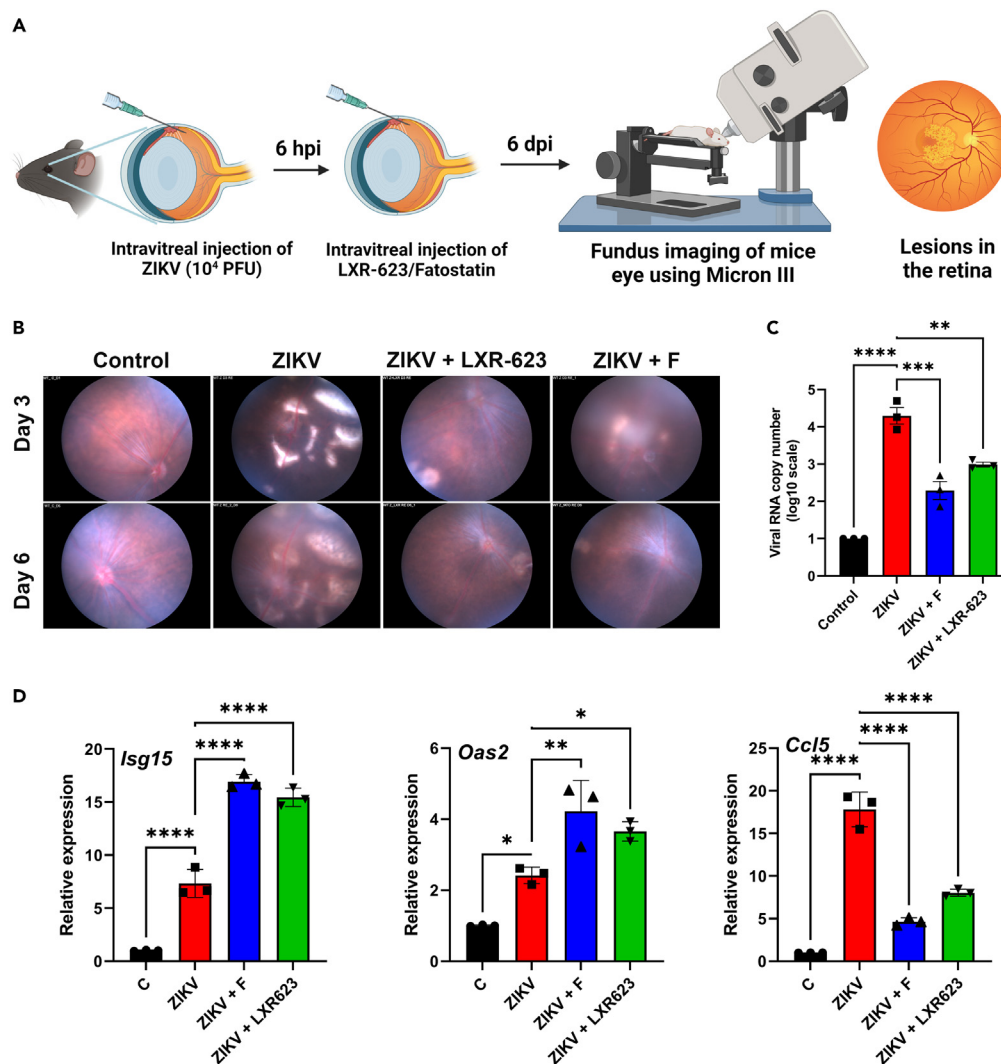
Figure 7. Treatment with LXR-623 and fatostatin reduces ZIKV induced chorioretinal lesions in mice eyes

(A) Schematic of experimental design involving intravitreal injection of ZIKV in C57/BL6 WT (4-to 6-week) mice eyes, intraocular injection of SREBP-2 inhibitor, fatostatin (F) or LXR agonist, LXR-623, followed by fundus imaging using Micron III system and quantification of viral RNA and antiviral immune genes in the retinal tissue.

(B) Representative funduscopic images showing the time course of retinal lesion/chorioretinal atrophy and RPE mottling in WT mice post ZIKV (10^4 PFU/eye).

(C) qPCR analysis of intracellular viral RNA in WT mouse retinas at day 6p.i. upon treatment with fatostatin or LXR623 as compared to mock-treated and ZIKV-infected mice eyes.

(D) qPCR was performed to quantify the relative expression of antiviral response genes (*Isg15*, *Oas2*, and *Ccl5*). The values represent mean ± SEM (n = 3), and the statistical analysis was performed using one-way ANOVA with Tukey's test. ****$p < 0.0001$, **$p < 0.01$, *$p < 0.05$.

potentially contributing to maintaining cellular cholesterol levels.[62] The inter-dependency of ABCG1 and SREBP-2 needs to be explored further to dissect their role during ZIKV infection.

In summary, our study demonstrates the role of ABCG1 and SREBP-2, the two arms of the cholesterol/lipid homeostasis pathway in regulating the innate antiviral response in RPE during ZIKV infection. Thus, ABCG1 and SREBP-2 regulated cholesterol homeostasis can be targeted to mount antiviral innate response during ocular ZIKV infection.

Limitations of the study

SREBP-2 is known to regulate the transcription of ABCG1 expression to maintain cholesterol homeostasis and vice-versa. However, their cross-talk during ZIKV infection has not been investigated in the present study. Also, the molecular mechanism of how ABCG1 and

SREBP-2 regulate antiviral innate immune response needs further investigation. Here, we primarily focused on cholesterol, the role of other lipids produced by the activation of SREBP-2 upon ZIKV infection also needs to be evaluated. The drugs were administered via intravitreal injections in our infection model; however, the systemic route of injection of the drugs for the treatment of ZIKV-induced retinal lesions would be interesting.

STAR★METHODS

Detailed methods are provided in the online version of this paper and include the following:

- KEY RESOURCES TABLE
- RESOURCE AVAILABILITY
  - Lead contact
  - Materials availability
  - Data and code availability
- EXPERIMENTAL MODEL AND STUDY PARTICIPANT DETAILS
  - Mice and ethics statement
  - Cells and virus strains
  - Mouse model of ZIKV-induced chorioretinal atrophy
- METHOD DETAILS
  - Immunofluorescence assay
  - RNA extraction and qPCR
  - Immunoblotting
  - Virus infection and plaque assay
  - Cell viability assay
  - Cholesterol efflux assay
  - Lipid droplet staining
  - Preprocessing and annotation of transcriptomic data
  - Transcriptomic data analysis
- QUANTIFICATION AND STATISTICAL ANALYSIS

SUPPLEMENTAL INFORMATION

Supplemental information can be found online at https://doi.org/10.1016/j.isci.2024.109088.

AUTHOR CONTRIBUTIONS

A.K. conceived the idea, designed the experiments, and provided direction and funding for the project. S.S. designed, performed the experiments, and prepared the figures, and S.S. and R.E.W. analyzed the data. S.S., V.A., and A.K. wrote the manuscript. S.G. helped with experimental design, provided intellectual inputs, and critically reviewed the manuscript. All authors contributed to the editing of the final manuscript.

DECLARATION OF INTERESTS

The authors declare no competing interests.

REFERENCES

1. Ventura, C.V., Maia, M., Bravo-Filho, V., Góis, A.L., and Belfort, R., Jr. (2016). Zika virus in Brazil and macular atrophy in a child with microcephaly. Lancet *387*, 228. https://doi.org/10.1016/S0140-6736(16)00006-4.

2. Oliveira Melo, A.S., Malinger, G., Ximenes, R., Szejnfeld, P.O., Alves Sampaio, S., and Bispo de Filippis, A.M. (2016). Zika virus intrauterine infection causes fetal brain abnormality and microcephaly: tip of the iceberg? Ultrasound Obstet. Gynecol. *47*, 6–7. https://doi.org/10.1002/uog.15831.

3. Miner, J.J., Cao, B., Govero, J., Smith, A.M., Fernandez, E., Cabrera, O.H., Garber, C., Noll, M., Klein, R.S., Noguchi, K.K., et al. (2016). Zika Virus Infection during Pregnancy in Mice Causes Placental Damage and Fetal Demise. Cell *165*, 1081–1091. https://doi.org/10.1016/j.cell.2016.05.008.

4. Miner, J.J., and Diamond, M.S. (2017). Zika Virus Pathogenesis and Tissue Tropism. Cell Host Microbe *21*, 134–142. https://doi.org/10.1016/j.chom.2017.01.004.

5. Ventura, L.O., Ventura, C.V., Lawrence, L., van der Linden, V., van der Linden, A., Gois, A.L., Cavalcanti, M.M., Barros, E.A., Dias, N.C., Berrocal, A.M., and Miller, M.T. (2017). Visual impairment in children with congenital Zika syndrome. J. Am. Assoc. Pediatric Ophthalmol. Strabismus *21*, 295–299.e2. https://doi.org/10.1016/j.jaapos.2017.04.003.

6. Sarno, M., Sacramento, G.A., Khouri, R., do Rosário, M.S., Costa, F., Archanjo, G., Santos, L.A., Nery, N., Vasilakis, N., Ko, A.I., and de Almeida, A.R.P. (2016). Zika Virus Infection and Stillbirths: A Case of Hydrops Fetalis, Hydranencephaly and Fetal Demise. PLoS Neglected Trop. Dis. *10*, e0004517. https://doi.org/10.1371/journal.pntd.0004517.

7. Miranda, H.A.d., 2nd, Costa, M.C., Frazão, M.A.M., Simão, N., Franchischini, S., and Moshfeghi, D.M. (2016). Expanded Spectrum of Congenital Ocular Findings in Microcephaly with Presumed Zika Infection. Ophthalmology *123*, 1788–1794. https://doi.org/10.1016/j.ophtha.2016.05.001.

8. Miranda-Filho, D.D.B., Martelli, C.M.T., Ximenes, R.A.D.A., Araújo, T.V.B., Rocha, M.A.W., Ramos, R.C.F., Dhalia, R., França, R.F.D.O., Marques Júnior, E.T.D.A., and Rodrigues, L.C. (2016). Initial Description of the Presumed Congenital Zika Syndrome. Am. J. Publ. Health *106*, 598–600. https://doi.org/10.2105/AJPH.2016.303115.

9. Ventura, C.V., Maia, M., Ventura, B.V., Linden, V.V.D., Araújo, E.B., Ramos, R.C., Rocha, M.A.W., Carvalho, M.D.C.G., Belfort, R., and Ventura, L.O. (2016). Ophthalmological findings in infants with microcephaly and presumable intra-uterus Zika virus infection. Arq. Bras. Oftalmol. *79*, 1–3. https://doi.org/10.5935/0004-2749.20160002.

10. de Paula Freitas, B., de Oliveira Dias, J.R., Prazeres, J., Sacramento, G.A., Ko, A.I., Maia, M., and Belfort, R., Jr. (2016). Ocular Findings in Infants With Microcephaly Associated With Presumed Zika Virus Congenital Infection in Salvador, Brazil. JAMA Ophthalmol. *134*, 529–535. https://doi.org/10.1001/jamaophthalmol.2016.0267.

11. Singh, S., and Kumar, A. (2018). Ocular Manifestations of Emerging Flaviviruses and the Blood-Retinal Barrier. Viruses *10*. https://doi.org/10.3390/v10100530.

12. Garcia, G., Jr., Paul, S., Beshara, S., Ramanujan, V.K., Ramaiah, A., Nielsen-Saines, K., Li, M.M.H., French, S.W., Morizono, K., Kumar, A., and Arumugaswami, V. (2020). Hippo Signaling Pathway Has a Critical Role in Zika Virus Replication and in the Pathogenesis of Neuroinflammation. Am. J. Pathol. *190*, 844–861. https://doi.org/10.1016/j.ajpath.2019.12.005.

13. Singh, P.K., Guest, J.M., Kanwar, M., Boss, J., Gao, N., Juzych, M.S., Abrams, G.W., Yu, F.S., and Kumar, A. (2017). Zika virus infects cells lining the blood-retinal barrier and causes chorioretinal atrophy in mouse eyes. JCI Insight *2*, e92340. https://doi.org/10.1172/jci.insight.92340.

14. Salinas, S., Erkilic, N., Damodar, K., Molès, J.P., Fournier-Wirth, C., Van de Perre, P., Kalatzis, V., and Simonin, Y. (2017). Zika Virus Efficiently Replicates in Human Retinal Epithelium and Disturbs Its Permeability. J. Virol. *91*, e02144-16. https://doi.org/10.1128/JVI.02144-16.

15. Singh, P.K., Khatri, I., Jha, A., Pretto, C.D., Spindler, K.R., Arumugaswami, V., Giri, S., Kumar, A., and Bhasin, M.K. (2018). Determination of system level alterations in host transcriptome due to Zika virus (ZIKV) Infection in retinal pigment epithelium. Sci. Rep. *8*, 11209. https://doi.org/10.1038/s41598-018-29329-2.

16. Lorizate, M., and Kräusslich, H.G. (2011). Role of Lipids in Virus Replication. Cold Spring Harbor Perspect. Biol. *3*, a004820.

17. Osuna-Ramos, J.F., Reyes-Ruiz, J.M., and Del Ángel, R.M. (2018). The Role of Host Cholesterol During Flavivirus Infection. Front. Cell. Infect. Microbiol. *8*, 388. https://doi.org/10.3389/fcimb.2018.00388.

18. Liu, S.Y., Aliyari, R., Chikere, K., Li, G., Marsden, M.D., Smith, J.K., Pernet, O., Guo, H., Nusbaum, R., Zack, J.A., et al. (2013). Interferon-inducible cholesterol-25-hydroxylase broadly inhibits viral entry by production of 25-hydroxycholesterol. Immunity *38*, 92–105. https://doi.org/10.1016/j.immuni.2012.11.005.

19. Zelcer, N., and Tontonoz, P. (2006). Liver X receptors as integrators of metabolic and inflammatory signaling. J. Clin. Invest. *116*, 607–614. https://doi.org/10.1172/JCI27883.

20. Villa, G.R., Hulce, J.J., Zanca, C., Bi, J., Ikegami, S., Cahill, G.L., Gu, Y., Lum, K.M., Masui, K., Yang, H., et al. (2016). An LXR-Cholesterol Axis Creates a Metabolic Co-Dependency for Brain Cancers. Cancer Cell *30*, 683–693. https://doi.org/10.1016/j.ccell.2016.09.008.

21. Griffett, K., Solt, L.A., El-Gendy, B.E.D.M., Kamenecka, T.M., and Burris, T.P. (2013). A liver-selective LXR inverse agonist that suppresses hepatic steatosis. ACS Chem. Biol. *8*, 559–567. https://doi.org/10.1021/cb300541g.

22. Inoue, K., and Imai, Y. (2015). Fatostatin, an SREBP inhibitor, prevented RANKL-induced bone loss by suppression of osteoclast differentiation. Biochim. Biophys. Acta *1852*, 2432–2441. https://doi.org/10.1016/j.bbadis.2015.08.018.

23. Ma, S., Murakami, K., Tanaka, K., Hashimoto, M., Tanaka, M., Kitagori, K., Akizuki, S., Nakashima, R., Yoshifuji, H., Ohmura, K., et al. (2022). Fatostatin ameliorates inflammation without affecting cell viability. FEBS Open Bio *12*, 594–604. https://doi.org/10.1002/2211-5463.13364.

24. Detrick, B., and Hooks, J.J. (2010). Immune regulation in the retina. Immunol. Res. *47*, 153–161. https://doi.org/10.1007/s12026-009-8146-1.

25. Simonin, Y., Erkilic, N., Damodar, K., Clé, M., Desmetz, C., Bolloré, K., Taleb, M., Torriano, S., Barthelemy, J., Dubois, G., et al. (2019). Zika virus induces strong inflammatory responses and impairs homeostasis and function of the human retinal pigment epithelium. EBioMedicine *39*, 315–331. https://doi.org/10.1016/j.ebiom.2018.12.010.

26. Tall, A.R., Yvan-Charvet, L., Terasaka, N., Pagler, T., and Wang, N. (2008). HDL, ABC transporters, and cholesterol efflux: implications for the treatment of atherosclerosis. Cell Metabol. *7*, 365–375. https://doi.org/10.1016/j.cmet.2008.03.001.

27. Yvan-Charvet, L., Wang, N., and Tall, A.R. (2010). Role of HDL, ABCA1, and ABCG1 transporters in cholesterol efflux and immune responses. Arterioscler. Thromb. Vasc. Biol. *30*, 139–143. https://doi.org/10.1161/ATVBAHA.108.179283.

28. Lai, L., Azzam, K.M., Lin, W.C., Rai, P., Lowe, J.M., Gabor, K.A., Madenspacher, J.H., Aloor, J.J., Parks, J.S., Näär, A.M., and Fessler, M.B. (2016). MicroRNA-33 Regulates the Innate Immune Response via ATP Binding Cassette Transporter-mediated Remodeling of Membrane Microdomains. J. Biol. Chem. *291*, 19651–19660. https://doi.org/10.1074/jbc.M116.723056.

29. Draper, D.W., Gowdy, K.M., Madenspacher, J.H., Wilson, R.H., Whitehead, G.S., Nakano, H., Pandiri, A.R., Foley, J.F., Remaley, A.T., Cook, D.N., and Fessler, M.B. (2012). ATP binding cassette transporter G1 deletion induces IL-17-dependent dysregulation of pulmonary adaptive immunity. J. Immunol. *188*, 5327–5336. https://doi.org/10.4049/jimmunol.1101605.

30. Fitzgerald, M.L., Mujawar, Z., and Tamehiro, N. (2010). ABC transporters, atherosclerosis and inflammation. Atherosclerosis *211*, 361–370. https://doi.org/10.1016/j.atherosclerosis.2010.01.011.

31. Out, R., Hoekstra, M., Habets, K., Meurs, I., de Waard, V., Hildebrand, R.B., Wang, Y., Chimini, G., Kuiper, J., Van Berkel, T.J.C., and Van Eck, M. (2008). Combined deletion of macrophage ABCA1 and ABCG1 leads to massive lipid accumulation in tissue macrophages and distinct atherosclerosis at relatively low plasma cholesterol levels. Arterioscler. Thromb. Vasc. Biol. *28*, 258–264. https://doi.org/10.1161/ATVBAHA.107.156935.

32. Mukherjee, S., Ghosh, R.N., and Maxfield, F.R. (1997). Endocytosis. Physiol. Rev. *77*, 759–803. https://doi.org/10.1152/physrev.1997.77.3.759.

33. Crouchet, E., Lefèvre, M., Verrier, E.R., Oudot, M.A., Baumert, T.F., and Schuster, C. (2017). Extracellular lipid-free apolipoprotein E inhibits HCV replication and induces ABCG1-dependent cholesterol efflux. Gut *66*, 896–907. https://doi.org/10.1136/gutjnl-2015-311289.

34. Hwang, J., Wang, Y., and Fikrig, E. (2019). Inhibition of Chikungunya Virus Replication in Primary Human Fibroblasts by Liver X Receptor Agonist. Antimicrob. Agents Chemother. *63*, e01220-19. https://doi.org/10.1128/AAC.01220-19.

35. Welsch, S., Miller, S., Romero-Brey, I., Merz, A., Bleck, C.K.E., Walther, P., Fuller, S.D.,

Antony, C., Krijnse-Locker, J., and Bartenschlager, R. (2009). Composition and three-dimensional architecture of the dengue virus replication and assembly sites. Cell Host Microbe 5, 365–375. https://doi.org/10.1016/j.chom.2009.03.007.

36. Neufeldt, C.J., Cortese, M., Acosta, E.G., and Bartenschlager, R. (2018). Rewiring cellular networks by members of the Flaviviridae family. Nat. Rev. Microbiol. 16, 125–142. https://doi.org/10.1038/nrmicro.2017.170.

37. Hong, C., and Tontonoz, P. (2014). Liver X receptors in lipid metabolism: opportunities for drug discovery. Nat. Rev. Drug Discov. 13, 433–444. https://doi.org/10.1038/nrd4280.

38. Howe, V., Sharpe, L.J., Alexopoulos, S.J., Kunze, S.V., Chua, N.K., Li, D., and Brown, A.J. (2016). Cholesterol homeostasis: How do cells sense sterol excess? Chem. Phys. Lipids 199, 170–178. https://doi.org/10.1016/j.chemphyslip.2016.02.011.

39. Venkateswaran, A., Laffitte, B.A., Joseph, S.B., Mak, P.A., Wilpitz, D.C., Edwards, P.A., and Tontonoz, P. (2000). Control of cellular cholesterol efflux by the nuclear oxysterol receptor LXR alpha. Proc. Natl. Acad. Sci. USA 97, 12097–12102. https://doi.org/10.1073/pnas.200367697.

40. Mujawar, Z., Rose, H., Morrow, M.P., Pushkarsky, T., Dubrovsky, L., Mukhamedova, N., Fu, Y., Dart, A., Orenstein, J.M., Bobryshev, Y.V., et al. (2006). Human immunodeficiency virus impairs reverse cholesterol transport from macrophages. PLoS Biol. 4, e365. https://doi.org/10.1371/journal.pbio.0040365.

41. Mlera, L., Offerdahl, D.K., Dorward, D.W., Carmody, A., Chiramel, A.I., Best, S.M., and Bloom, M.E. (2021). The liver X receptor agonist LXR 623 restricts flavivirus replication. Emerg. Microb. Infect. 10, 1378–1389. https://doi.org/10.1080/22221751.2021.1947749.

42. Yu, S., Li, S., Henke, A., Muse, E.D., Cheng, B., Welzel, G., Chatterjee, A.K., Wang, D., Roland, J., Glass, C.K., and Tremblay, M. (2016). Dissociated sterol-based liver X receptor agonists as therapeutics for chronic inflammatory diseases. Faseb. J. 30, 2570–2579. https://doi.org/10.1096/fj.201600244R.

43. Pascual-García, M., Rué, L., León, T., Julve, J., Carbó, J.M., Matalonga, J., Auer, H., Celada, A., Escolà-Gil, J.C., Steffensen, K.R., et al. (2013). Reciprocal negative cross-talk between liver X receptors (LXRs) and STAT1: effects on IFN-gamma-induced inflammatory responses and LXR-dependent gene expression. J. Immunol. 190, 6520–6532. https://doi.org/10.4049/jimmunol.1201393.

44. Zeng, J., Wu, D., Hu, H., Young, J.A.T., Yan, Z., and Gao, L. (2020). Activation of the Liver X Receptor Pathway Inhibits HBV Replication in Primary Human Hepatocytes. Hepatology 72, 1935–1948. https://doi.org/10.1002/hep.31217.

45. Cloherty, A.P.M., Olmstead, A.D., Ribeiro, C.M.S., and Jean, F. (2020). Hijacking of Lipid Droplets by Hepatitis C, Dengue and Zika Viruses-From Viral Protein Moonlighting to Extracellular Release. Int. J. Mol. Sci. 21, 7901. https://doi.org/10.3390/ijms21217901.

46. Horton, J.D., Goldstein, J.L., and Brown, M.S. (2002). SREBPs: activators of the complete program of cholesterol and fatty acid synthesis in the liver. J. Clin. Invest. 109, 1125–1131. https://doi.org/10.1172/JCI15593.

47. DeBose-Boyd, R.A., and Ye, J. (2018). SREBPs in Lipid Metabolism, Insulin Signaling, and Beyond. Trends Biochem. Sci. 43, 358–368. https://doi.org/10.1016/j.tibs.2018.01.005.

48. Olmstead, A.D., Knecht, W., Lazarov, I., Dixit, S.B., and Jean, F. (2012). Human subtilase SKI-1/S1P is a master regulator of the HCV Lifecycle and a potential host cell target for developing indirect-acting antiviral agents. PLoS Pathog. 8, e1002468. https://doi.org/10.1371/journal.ppat.1002468.

49. Hyrina, A., Meng, F., McArthur, S.J., Eivemark, S., Nabi, I.R., and Jean, F. (2017). Human Subtilisin Kexin Isozyme-1 (SKI-1)/Site-1 Protease (S1P) regulates cytoplasmic lipid droplet abundance: A potential target for indirect-acting anti-dengue virus agents. PLoS One 12, e0174483. https://doi.org/10.1371/journal.pone.0174483.

50. Peña, J., and Harris, E. (2012). Early dengue virus protein synthesis induces extensive rearrangement of the endoplasmic reticulum independent of the UPR and SREBP-2 pathway. PLoS One 7, e38202. https://doi.org/10.1371/journal.pone.0038202.

51. Branche, E., Wang, Y.T., Viramontes, K.M., Valls Cuevas, J.M., Xie, J., Ana-Sosa-Batiz, F., Shafee, N., Duttke, S.H., McMillan, R.E., Clark, A.E., et al. (2022). SREBP2-dependent lipid gene transcription enhances the infection of human dendritic cells by Zika virus. Nat. Commun. 13, 5341. https://doi.org/10.1038/s41467-022-33041-1.

52. Mackenzie, J.M., Khromykh, A.A., and Parton, R.G. (2007). Cholesterol manipulation by West Nile virus perturbs the cellular immune response. Cell Host Microbe 2, 229–239. https://doi.org/10.1016/j.chom.2007.09.003.

53. Rothwell, C., Lebreton, A., Young Ng, C., Lim, J.Y.H., Liu, W., Vasudevan, S., Labow, M., Gu, F., and Gaither, L.A. (2009). Cholesterol biosynthesis modulation regulates dengue viral replication. Virology 389, 8–19. https://doi.org/10.1016/j.virol.2009.03.025.

54. Merino-Ramos, T., Jiménez de Oya, N., Saiz, J.C., and Martín-Acebes, M.A. (2017). Antiviral Activity of Nordihydroguaiaretic Acid and Its Derivative Tetra-O-Methyl Nordihydroguaiaretic Acid against West Nile Virus and Zika Virus. Antimicrob. Agents Chemother. 61, e00376-17. https://doi.org/10.1128/AAC.00376-17.

55. Kusnadi, A., Park, S.H., Yuan, R., Pannellini, T., Giannopoulou, E., Oliver, D., Lu, T., Park-Min, K.H., and Ivashkiv, L.B. (2019). The Cytokine TNF Promotes Transcription Factor SREBP Activity and Binding to Inflammatory Genes to Activate Macrophages and Limit Tissue Repair. Immunity 51, 241–257.e9. https://doi.org/10.1016/j.immuni.2019.06.005.

56. Cerqueira, N.M.F.S.A., Oliveira, E.F., Gesto, D.S., Santos-Martins, D., Moreira, C., Moorthy, H.N., Ramos, M.J., and Fernandes, P.A. (2016). Cholesterol Biosynthesis: A Mechanistic Overview. Biochemistry 55, 5483–5506. https://doi.org/10.1021/acs.biochem.6b00342.

57. Ikonen, E. (2008). Cellular cholesterol trafficking and compartmentalization. Nat. Rev. Mol. Cell Biol. 9, 125–138. https://doi.org/10.1038/nrm2336.

58. Crofford, O.B. (1995). N. Engl. J. Med. 333, 588–589. https://doi.org/10.1056/NEJM199508313330910.

59. Singh, S., Singh, P.K., Suhail, H., Arumugaswami, V., Pellett, P.E., Giri, S., and Kumar, A. (2020). AMP-Activated Protein Kinase Restricts Zika Virus Replication in Endothelial Cells by Potentiating Innate Antiviral Responses and Inhibiting Glycolysis. J. Immunol. 204, 1810–1824. https://doi.org/10.4049/jimmunol.1901310.

60. Aryal, B., Singh, A.K., Rotllan, N., Price, N., and Fernández-Hernando, C. (2017). MicroRNAs and lipid metabolism. Curr. Opin. Lipidol. 28, 273–280. https://doi.org/10.1097/MOL.0000000000000420.

61. Lee, W., Ahn, J.H., Park, H.H., Kim, H.N., Kim, H., Yoo, Y., Shin, H., Hong, K.S., Jang, J.G., Park, C.G., et al. (2020). COVID-19-activated SREBP2 disturbs cholesterol biosynthesis and leads to cytokine storm. Signal Transduct. Targeted Ther. 5, 186. https://doi.org/10.1038/s41392-020-00292-7.

62. Marquart, T.J., Allen, R.M., Ory, D.S., and Baldán, A. (2010). miR-33 links SREBP-2 induction to repression of sterol transporters. Proc. Natl. Acad. Sci. USA 107, 12228–12232. https://doi.org/10.1073/pnas.1005191107.

63. Dunn, K.C., Aotaki-Keen, A.E., Putkey, F.R., and Hjelmeland, L.M. (1996). ARPE-19, a human retinal pigment epithelial cell line with differentiated properties. Exp. Eye Res. 62, 155–169. https://doi.org/10.1006/exer.1996.0020.

STAR★METHODS

KEY RESOURCES TABLE

REAGENT or RESOURCE	SOURCE	IDENTIFIER
Antibodies		
Anti-ABCG1 Mouse mAb (2E11)	Millipore	Cat#ST1606; RRID: AB_10682907
Purified Mouse Anti-SREBP-2	BD Pharmingen	Cat#557037; RRID: AB_396560
Anti-β-Actin antibody, Mouse monoclonal	Sigma-Aldrich	Cat#A1978; RRID: AB_476692
Zika virus NS3 protein antibody	GeneTex	Cat#GTX133309; RRID: AB_2756864
Bacterial and virus strains		
Zika virus: PRVABC59	BEI repository	Cat#NR-50684
ABCG1 lentivirus	SantaCruz Biotechnologies	Cat#sc-41138-V
SREBP-2 lentivirus	SantaCruz Biotechnologies	Cat#sc-36559-V
Chemicals, peptides, and recombinant proteins		
TRizol reagent	Life Technologies	Cat#15596018
FBS (Fetal Bovine Serum)	CPS Serum	Cat#FBS-500-HI
Fatostatin	Cayman chemical	Cat#13562
LXR-623	Cayman chemical	Cat#21117
SR-9238	Cayman chemical	Cat#18771
Critical commercial assays		
Micro BCA Protein Assay kit	Thermo Fisher Scientific	Cat#23235
Supersignal West Femto Maximum Sensitivity Substrate	Thermo Fisher Scientific	Cat#34096
Maxima First strand cDNA synthesis kit for RT-qPCR	Thermo Fisher Scientific	Cat#K1641
Radiant Green HiROX qPCR kit	Alkali Scientific	Cat#QS2050
Deposited data		
RNA sequencing data	NCBI	PRJNA1032054
Experimental models: Cell lines		
ARPE-19 cell line	ATCC	Cat#CRL-2302
Primary RPE cells	Lonza	Cat#00194987
Experimental models: Organisms/strains		
Mouse: C57/BL6J	The Jackson Laboratory	https://www.jax.org/strain/000664
Software and algorithms		
Prism 9	GraphPad	https://www.graphpad.com
R version 3.6.3	R project	https://www.r-project.org/

RESOURCE AVAILABILITY

Lead contact

Further information and requests for resources and reagents should be directed to and will be fulfilled by the lead contact, Ashok Kumar (akuma@med.wayne.edu).

Materials availability

This study did not generate new unique reagents.

Data and code availability

- All data reported in this paper will be shared by the lead contact upon request.
- The transcriptomics data generated from this study is deposited in the NIH Sequence Read Archive (SRA) data. The accession number for the raw data is PRJNA1032054 (https://dataview.ncbi.nlm.nih.gov/object/PRJNA1032054?reviewer=8tpoe62pk8l8rrmrcsjgu2656g).
- Any additional information required to reanalyze the data reported in this paper is available from the lead contact upon request.

EXPERIMENTAL MODEL AND STUDY PARTICIPANT DETAILS

Mice and ethics statement

Wild-type (WT) C57BL/6 mice (both male and female, aged 6-8 weeks) were purchased from the Jackson Laboratory and/or bred in-house in the Division of Laboratory Animal Resources facility at Kresge Eye Institute. Mice were maintained in a 12h light/dark cycle at 22°C and fed LabDiet rodent chow (Labdiet Pico lab Laboratory, St Louis, MO) and water *ad libitum*. All experimental procedures were performed in compliance with the Animals in Ophthalmic and Vision Research (ARVO) statement for the use of animals and were approved by the institutional animal care and use committee (IACUC) of Wayne State University.

Cells and virus strains

Primary human retinal pigment epithelial cells (Pr. RPE) were grown in RtEBM media (Lonza) supplemented with growth factors and 2% FBS. Human retinal pigment epithelial ARPE-19 cell line (ATCC CRL-2302), derived from normal eyes of a 19-year old male who died from head trauma in a motor vehicle accident[63] was grown in DMEM/F12 media (Invitrogen) and Vero cells were grown in Dulbecco's minimal essential medium (DMEM, Invitrogen) complemented with 10% Fetal bovine serum (FBS), respectively with 1% penicillin-streptomycin (P/S) solution (Invitrogen). Cells were grown at 37°C in 5% CO_2 with 95% humidity (Fisherbrand).

Zika virus strain PRVABC59 (NR-50240), initially isolated from human blood in Puerto Rico in December 2015 was acquired through BEI Resources, National Institute of Allergy and Infectious Diseases (NIAID), NIH.

Mouse model of ZIKV-induced chorioretinal atrophy

Mice were injected with ZIKV (∼1×10^4 PFU/eye) intravitreally in the right eye. The contralateral eyes were injected with the vehicle and served as mock control. The drugs were administered 6 hours post-infection using the same site of injection. At the desired time points after infection, funduscopic analysis was performed using Micron III (Phoenix Research Lab). The animals were then euthanized, and enucleated eyes were subjected to viral burden estimation by plaque assay while the retinal tissue was used for inflammatory cytokine/chemokine assays and viral RNA quantification as described in the following sections.

METHOD DETAILS

Immunofluorescence assay

Cells were seeded in four-well chamber slides (Fisher Scientific) and infected with ZIKV at MOI 1 at 90% confluency. The cells were fixed with 4% paraformaldehyde in 1X PBS overnight at 4°C and washed thrice with 1X PBS. The cells permeabilized and blocked using 1% BSA, and 0.4% Triton X-100 in 1X PBS for 1 hour at room temperature. The cells were then incubated with primary antibody (mouse anti-Flavivirus 4G2 IgG (1:100), anti-ABCG1 (1:100), anti-SREBP2 (1:100)) in the dilution buffer in a humidified chamber overnight at 4°C followed by three washes with 1X PBS. The cells were incubated with secondary antibodies (anti-mouse Alexa Fluor 594, anti-rabbit Alexa Fluor 594, and anti-goat Alexa Fluor 594, Invitrogen) for 1 hour at room temperature in a humidified chamber followed by three washes with 1X PBS and mounted in Vectashield anti-fade mounting medium (Vector Laboratories). The cells were visualized using the Keyence fluorescence microscope (Nikon).

RNA extraction and qPCR

Total cellular RNA was extracted from the RPE cells and mice retinal tissue infected and treated with the drugs/shRNA-lentivirus as specified using Trizol (Invitrogen) reagent as per the manufacturer's instructions. The cDNA was prepared using 1 μg of total RNA using a Maxima First Strand cDNA Synthesis kit (Thermo Scientific) according to the manufacturer's directions. qRT-PCR was performed using gene-specific primers using a StepOnePlus Real-time PCR system (Applied Biosystems). Quantification of gene expression was determined via the comparative $^{\Delta\Delta}CT$ method and expressed as relative expression.

The viral RNA transcripts were measured using a TaqMan probe–based qRT-PCR assay to detect the ZIKV envelope gene by plotting a standard curve produced using serial 10-fold dilutions of ZIKV RNA as described previously (57, 64, 65) on a StepOnePlus Real-Time PCR system (Applied Biosystems). The viral RNA was expressed as $\log_{10}$ viral RNA copies/ug of total RNA. The viral copy number was calculated with reference to the house-keeping gene GAPDH to assess viral replication per cell.

Immunoblotting

For immunoblotting analysis, cells were lysed in RIPA lysis buffer (Thermo Scientific), and the protein concentration was quantified using a BCA assay kit (Thermo Scientific) as per the manufacturer's instructions. The whole cell denatured proteins were resolved on 10% SDS-PAGE (sodium dodecyl sulfate-polyacrylamide gel electrophoresis) and transferred onto 0.45 μm nitrocellulose membranes (Bio-Rad,

Hercules, CA). The nitrocellulose membrane was blocked with 5% non-fat skim milk followed by a wash with 1X TBST (Tris-glycine buffer with 0.5% Tween 20). Blots were incubated with the primary antibody in 5% BSA overnight at 4°C with shaking. Membranes were then washed thrice with 1X TBST followed by incubation with the secondary antibody at room temperature for two hours. The membrane was then washed thrice with 1X TBST and the protein bands were visualized using Supersignal West Femto chemiluminescent substrate (Thermo Scientific, Rockford, IL). The densitometry values were obtained using ImageJ software.

Virus infection and plaque assay

The RPE cells were seeded at 70–80% confluence at 37°C in a humidified CO_2 incubator. Cells were washed with 1X PBS and infected with ZIKV at a multiplicity of infection (MOI) of 1 or mock-infected in serum-free media. The cells were incubated with the virus for 2h with intermittent shaking every 15 min. The culture medium was removed and complemented with DMEM/F12 media with 2% FBS (Fetal bovine serum) and 1% P/S solution for the preferred period of incubation time. The cell culture supernatant was collected at different time points for the estimation of virus titer by plaque assay.

For plaque assay, Vero cells were seeded at the confluence in 12-well tissue culture plates and washed once with 1X PBS after adherence. Serial dilutions of culture supernatants were prepared in serum-free DMEM media and added to the cells for 2 hours. The virus media was removed, and an equal mixture of 2X EMEM and 2% CMC (Carboxymethyl cellulose) was added onto the monolayer and incubated for 5 days (37°C in a CO_2 incubator with humidity). The cell monolayer was fixed with 4% paraformaldehyde (PFA) for 4 to 6 hours followed by careful removal of the solution and the overlay media. The cells were stained using a crystal violet solution for 4 to 6 hours and washed with distilled water to visualize the plaques. The plaques were counted, and the viral titer was expressed as log_{10} PFU/ml. The experiment was conducted in triplicates and represented with statistical analysis.

Cell viability assay

The RPE cells were treated with the drugs at different concentrations and incubated for 48h followed by MTT (3-(4,5-dimethylthiazol-2-yl)-2,5-diphenyl tetrazolium bromide) assay. Briefly, the MTT reagent (0.5mg/mL), in the cell culture medium was added to the cells for 4 hours followed by lysis of the cells using 20% SDS (Sodium dodecyl sulfate) in 50% DMF (Dimethylformamide) solution. The readings were collected at 570nm and the values were plotted with reference to the untreated control as cell viability (%).

Cholesterol efflux assay

The RPE cells were seeded onto the 96-well plates and upon 80% confluency, the cholesterol efflux assay was performed as per the manufacturer's instructions (Abcam). Briefly, the cells were allowed to attach to the wells for 4 to 6 post seeding followed by a PBS wash to remove the media. The labeling medium was added to the wells (1:1 volume of labeling media and RPMI media serum-free) for an hour followed by the addition of equilibration media (1:1 volume of equilibration media and RPMI serum-free) overnight. The cells were treated with virus infection and/or drugs for 24 hours post-infection. The supernatant was transferred to a white 96-well plate and the fluorescence was measured at an excitation/emission of 485/523 nm. Similarly, the cells were lysed using cell lysis buffer followed by 30 minutes of incubation along with shaking. The cell lysate was transferred to a white 96-well plate and the fluorescence was measured. The net % cholesterol efflux was measured as per the manufacturer's provided equation: % cholesterol efflux = RFU of supernatant / ((RFU of cell lysate + RFU of supernatant) *100).

Lipid droplet staining

The RPE cells were seeded onto 4 well chamber slides and were infected with ZIKV at 90% confluency. The cells were washed with 1X PBS followed by the addition of BioTracker 488 Green Lipid Droplet dye (EMD Millipore Sigma) for the live staining of cells (1:1000 dilution in 1X PBS) for 30 minutes. The cells were visualized using a Keyence fluorescence microscope (Nikon).

Preprocessing and annotation of transcriptomic data

For transcriptomic data analysis, the original Affymetrix data was pre-processed using an oligo R package and later normalized and log-transformed using a multi-array average (RMA) method. Further, the CDF package was used for probe annotation of Affymetrix data. The probes of the normalized data were successfully mapped to Entrez Gene IDs and Gene Symbols by annotation package (annotate) in R. Wherever multiple probes matched a single gene symbol, we calculated the median values of those probes as the expression value for that gene.

Transcriptomic data analysis

For Affymetrix gene expression data, all statistical analyses were performed using the multiple R Bioconductor packages (http://www.Bioconductor.org). For analysis, the P-values were adjusted for multiple testing with Benjamini and Hochberg's method to control for false discovery rate (FDR). Probe sets showing at least a $\pm$ 2.5-fold change and an FDR < 0.05 were considered significant for the analysis. ggplot2 was used to generate the plots, and R package heatmap.2 was used for heatmap generation from fold changes value.

QUANTIFICATION AND STATISTICAL ANALYSIS

The data used in the study have been expressed as mean $\pm$ SD for cell-based assays while the animal tissue-based studies have been expressed as mean $\pm$ SEM. Statistical differences between the experimental groups were calculated using Graph Pad Prism 8.1 software. A value of $p < 0.05$ was considered statistically significant. All experiments were performed at least three times unless mentioned otherwise.